The Journal of Immunology

Essential Role of Canonical NF-κB Activity in the Development of Stromal Cell Subsets in Secondary Lymphoid Organs

Dana Bogdanova, Arata Takeuchi, Madoka Ozawa, Yasuhiro Kanda, M. Azizur Rahman, Burkhard Ludewig, Tatsuo Kinashi and Tomoya Katakai

J Immunol published online 5 November 2018
http://www.jimmunol.org/content/early/2018/11/02/jimmunol.1800539

Supplementary Material **http://www.jimmunol.org/content/suppl/2018/11/03/jimmunol.1800539.DCSupplemental**

The Journal of Immunology is published twice each month by The American Association of Immunologists, Inc., 1451 Rockville Pike, Suite 650, Rockville, MD 20852

Print ISSN: 0022-1767 Online ISSN: 1550-6606.

Published November 5, 2018, doi:10.4049/jimmunol.1800539

Essential Role of Canonical NF-κB Activity in the Development of Stromal Cell Subsets in Secondary Lymphoid Organs

Dana Bogdanova,* Arata Takeuchi,* Madoka Ozawa,* Yasuhiro Kanda,* M. Azizur Rahman,* Burkhard Ludewig,† Tatsuo Kinashi,‡ and Tomoya Katakai*

Organized tissue structure in the secondary lymphoid organs (SLOs) tightly depends on the development of fibroblastic stromal cells (FSCs) of mesenchymal origin; however, the mechanisms of this relationship are poorly understood. In this study, we specifically inactivated the canonical NF-κB pathway in FSCs in vivo by conditionally inducing IκBα mutant in a *Ccl19-IκBSR* mouse system in which NF-κB activity is likely to be suppressed in fetal FSC progenitors. Given that NF-κB activation in fetal FSCs is essential for SLO development, the animals were expected to lack SLOs. However, all SLOs were preserved in *Ccl19-IκBSR* mice. Instead, the T cell area was severely disturbed by the lack of CCL21-expressing FSCs, whereas the follicles and associated FSC networks were formed. Fate mapping revealed that IκBSR-expressing cells constituted only a small fraction of stromal compartment outside the follicles. Taken together, our findings indicate an essential role of the canonical NF-κB pathway activity in the development of three FSC subsets common to SLOs and suggest transient or stochastic CCL19 expression in FSC progenitors and a compensatory differentiation program of follicular FSCs. *The Journal of Immunology*, 2018, 201: 000–000.

Secondary lymphoid organs (SLOs) develop through complex processes of intimate interactions between lymphoid cells and nonhematopoietic stromal cells (1, 2). The interplay of lymphoid tissue inducer cells, an innate lymphoid cell population, with mesenchymal lymphoid tissue organizer (LTo) cells in fetal anlagen is necessary for the formation of lymph nodes (LNs) and Peyer's patches (PPs) (3–6), whereas the organization of white pulps in the spleen involves postnatal collaboration of mature lymphocytes and perivascular stromal cells (7, 8). In these cellular processes, lymphotoxin (LT) α1β2 and LTβR, which are displayed on lymphoid cells and mesenchymal cells, respectively, and the activation of NF-κB transcription factors via the canonical (RelA/p50 complex) and noncanonical (RelB/p52 complex) pathways are believed to play the key roles; gene deficiencies of these signaling mediators lead to the absence or malformation of SLOs (1, 9–12). In particular, NF-κB is required for the expression of chemokines such as CXCL13, CCL19, and CCL21, which recruit lymphoid cells to SLOs (11–16). However, in a strict sense, it has not been proven directly that NF-κB activity in LTo cells or mesenchymal progenitors itself is essential for the development and tissue organization of SLOs in vivo. Recent studies have suggested the presence of other complicated cellular interactions involving endothelial compartments in LN formation and distinct organ-specific development programs (8, 17).

In adult SLOs, B and T cells are clearly segregated in the follicles and T cell area. Different types of fibroblastic stromal cells (FSCs) that form intricate networks support each of the regions by providing a structural backbone (18). Follicular dendritic cells (FDCs) and marginal reticular cells (MRCs) in the center and outer part of the follicle, respectively, produce CXCL13 that regulates B cell localization and motility (19–21). MRCs, which display characteristics similar to those of LTo cells, such as the expression of RANKL and MAdCAM-1, have been shown to be FDC precursors (21–23). In T cell area, T zone reticular cells (TRCs), also known as fibroblastic reticular cells, produce CCL19 and CCL21, affecting the localization and migration of T cells and dendritic cells (24–27). These three stromal cell subsets are common to all types of SLOs and are considered to originate from a common mesenchymal progenitor (17, 28, 29).

The factors required for the development of FDCs are well studied, as this stromal cell type is absent in mice engineered to lack some immune system–related genes (10, 30). In particular, signals through LTβR and TNFR together with subsequent NF-κB activation play critical roles in the differentiation and maintenance of FDC network in the follicles (16, 31, 32). In contrast, the developmental processes of MRCs and TRCs remain poorly understood. Moreover, the mechanisms that regulate the generation of FSC subsets may possibly differ between SLO types, although it could not be verified in animals that completely lack LNs and PPs (e.g., in the cases of deficiencies in NF-κB components).

Ccl19-Cre BAC transgenic mouse strain is a useful tool for conditional gene targeting and fate mapping in FSC lineages

*Department of Immunology, Niigata University Graduate School of Medical and Dental Sciences, Niigata 951-8510, Japan; †Institute of Immunobiology, CH-9007 St. Gallen, Switzerland; and ‡Department of Molecular Genetics, Institute of Biomedical Science, Kansai Medical University, Hirakata, Osaka 573-1010, Japan

ORCIDs: 0000-0003-0412-533X (A.T.); 0000-0001-5026-2306 (M.O.); 0000-0001-8131-8130 (Y.K.); 0000-0002-7685-573X (B.L.); 0000-0002-4290-7028 (T. Katakai).

Received for publication April 16, 2018. Accepted for publication October 11, 2018.

This work was supported by Grant-in-Aid for Scientific Research on Innovative Areas 24111005 and Grant-in-Aid for Scientific Research Scientific Research (B) 16H05204 from the Ministry of Education, Culture, Sports, Science and Technology–Japan Society for the Promotion of Science (both to T. Katakai).

Address correspondence and reprint requests to Prof. Tomoya Katakai, Department of Immunology, Graduate School of Medical and Dental Sciences, Niigata University, 1-757 Asahimachi-dori, Chuo-ku, Niigata 951-8510, Japan. E-mail address: katakai@med.niigata-u.ac.jp

The online version of this article contains supplemental material.

Abbreviations used in this article: *Ccl19-EYFP*, *Ccl19-Cre/R26-stop^{flox}-EYFP*; FDC, follicular dendritic cell; FSC, fibroblastic stromal cell; HEV, high endothelial venule; LN, lymph node; LT, lymphotoxin; LTo, lymphoid tissue organizer; MRC, marginal reticular cell; PP, Peyer's patch; SLO, secondary lymphoid organ; TRC, T zone reticular cell.

during SLO development because LTo cells in fetal anlagen or postnatal progenitors express Cre recombinase driven by the *Ccl19* gene (8, 33). A mutant form of IκBα, IκBSR, is resistant to the degradation upon signaling; it strongly inhibits the activation of the canonical NF-κB pathway (34), which in turn suppresses the expression of noncanonical pathway components. Thus, IκBSR potentially inhibits both pathways (15). In this study, to assess the consequences of in vivo inactivation of the canonical NF-κB pathway specific to FSCs in SLOs, we generated a mouse in which both IκBSR and EGFP are conditionally induced under the control of the *Ccl19-Cre* locus. Characteristic structural alterations of SLOs in these animals prompted us to address the cause of these abnormalities. Fate mapping using bicistronic EGFP expression permitted the identification of IκBSR-expressing cells in situ, which allowed us to elucidate the indispensable role of the canonical NF-κB pathway activity in the development of FSC subsets and suggested the presence of unique differentiation programs.

Materials and Methods

Mice

C57BL/6JJcl mice were purchased from CLEA Japan. *Ccl19-Cre* [*Tg(Ccl19-cre)^{489Biat}*] and *R26-stop^{flox}-EYFP*[B6.129 × 1-*Gt(ROSA) 26Sor$^{tm1(EYFP)Cos}$*/J] mice were described previously (33). Mice were maintained under specific pathogen-free conditions in the animal facility of the Niigata University. All animal procedures were approved by the Committee on Animal Research at the Niigata University.

Murine IκBα cDNA was amplified from LN total RNA by RT-PCR using the following primers: 5′-TTAGATCTATGTTTCAGCCAGCTGGGCA-3′ and 5′-TTGCGGCCGCTTATAATGTCAGACGCTGGC-3′. To generate IκBSR, phosphorylation-resistant mutations (S32A/S36A) were introduced into the cloned cDNA by stepwise PCR using the above primers and following primers: 5′-CCTTCATGGCGTCCAGGCCGGCGTCGTGGC-3′ and 5′-GCCACGACGCCGGCCTGGACGCCATGAAGG-3′. *R26-stop^{flox}-IκBSR* mice were generated by knocking a targeting construct that contained CAG promoter, a reverse-oriented Neo^r cassette, transcription termination signal held between two loxP sites (*stop^{flox}*), and a bicistronic gene cassette encoding *IκBSR-ires-EGFP*, into the *Rosa26* locus, as described previously (35). The linearized construct was electroporated into C57BL/6J mouse primary embryonic stem cells, and G418-resistant colonies were screened by Southern blotting of genomic DNA using a Neo^r-flanking probe. *R26-stop^{flox}-IκBSR* mice were crossed with *Ccl19-Cre* mice to obtain *Ccl19-IκBSR* animals that were heterozygous for the *Ccl19-Cre* allele and homozygous for the *R26-stop^{flox}-IκBSR* allele. Mice of 8–12 wk of age were used for experiments. Homozygous *R26-stop^{flox}-IκBSR* mice were used as controls.

Abs

Primary Abs against the following proteins were used: CD3e (145-2C11), B220 (RA3-6B2), PNAd (MECA-79), MAdCAM-1 (MECA-367), CD45 (30-F11), CD31 (390), and podoplanin (8.1.1) (eBioscience); desmin (Abcam); CD35 (8C12) (BD Biosciences); VCAM-1 (BAF643), RANKL (BAF462), CCL21 (BAF457), CXCL13 (BAF470), and LYVE-1 (BAF2125) (R&D Systems); GFP (598) (MBL); Cre (D7L7L) (Cell Signaling). For secondary reagents, PE-, allophycocyanin-, AlexaFluor 488–, 546–, 555–, 594–, or 633–conjugated streptavidin, anti-rabbit IgG, and anti-rat IgG were purchased from Molecular Probes.

Flow cytometry

Single-cell suspensions were prepared from excised SLOs and stained with the Abs. To analyze stromal cells, LNs were digested with 1 mg/ml collagenase D and 0.1 mg/ml DNase I (Roche) as described (36) and stained with Abs against CD45, CD31, and podoplanin. Data were acquired using a FACSCalibur (BD Biosciences) flow cytometer and analyzed with CellQuest (BD Biosciences) or FlowJo software.

Immunohistochemistry

SLOs were fixed with 0.05% phosphate buffer containing 0.075 M L-lysine (pH 7.4), 0.01 M $NaIO_4$, and 1% paraformaldehyde at 4°C for 16–24 h. After fixation, LNs were equilibrated gradually with 10, 20, and 30% sucrose in PBS at 4°C, embedded in OCT compound (Sakura), and frozen at −80°C. Frozen sections (10 μm) were stained with Abs and mounted with Permafluor (Thermo Fisher Scientific). The specimens were examined using an LSM710 (Carl Zeiss) or an FV1200 (Olympus) confocal microscope. Digital images were prepared using Adobe Photoshop CS6 software.

For whole-mount immunohistochemistry, excised organs were fixed with 1% paraformaldehyde in PBS overnight at 4°C, and endogenous peroxidase activity was blocked with 0.3% H_2O_2 and 40% methanol in PBS overnight at 4°C. The specimens were permeabilized with 0.3% Triton X-100 in PBS at 4°C for 1.5 h followed by blocking with 1% BSA in PBST (0.05% Tween-20 in PBS) at 4°C for 2 h. The specimens were then incubated with 2 μg/ml biotin–anti-B220 Ab (eBioscience) in 1% BSA in PBST overnight at 4°C. Biotinylated Ab was detected using Vectastain ABC Kit and DAB Substrate Kit (Vector).

Quantitative RT-PCR analysis

Total RNA was extracted from SLOs using an RNeasy Mini kit (QIAGEN) or TRIzol reagent (Invitrogen), and cDNA was synthesized using the Superscript III First-Strand Synthesis System (Invitrogen). Quantitative PCR was performed using the LightCycler FastStart DNA Master^{PLUS} SYBR Green I (Roche) on a LightCycler (Roche). Primers used were as follows: *Cxcl13*, 5′-TGGCTGCCCCAAAACTGA-3′ and 5′-TGGCACGAGGATTCACACAT-3′; *Ccl19*, 5′-CTGCCTCAGATTATCTGCCAT-3′ and 5′-AGGTAGCGGAAGGCTTTCAC-3′; *Ccl21a*, 5′-ATCCCGGCAATCCTGTTCTC-3′ and 5′-GGTTCTGCACCCAGCCTTC-3′; *Des*, 5′-GTGGATGCAGCCACTCTAGC-3′ and 5′-TTAGCCGCGATGGTCTCATAC-3′; *Gapdh*, 5′-GCCAAGGTCATCCATGACAACT-3′ and 5′-GAGGGGCCATCCACAGTCTT-3′. The value was normalized to expression level of the *Gapdh* gene.

Stromal cell culture

The spleen was digested with 1 mg/ml collagenase D, 0.02 mg/ml Liberase TM, and 0.05 mg/ml DNase I (Roche). The CD45$^-$ stromal cell fraction was enriched from the cell suspension by magnetic cell sorting using microbeads-conjugated anti-CD45 Ab (Miltenyi) and biotin–anti-CD31 Ab (eBioscience) followed by microbeads-conjugated anti-biotin Ab (Miltenyi). Cells were suspended in 10% FCS DMEM medium supplemented with penicillin and streptomycin and cultured in 24-well plates coated with gelatin (0.3% in PBS, overnight at 37°C) for 4–6 d. Semiconfluent cells were stimulated without or with 20 ng/ml TNF-α (PeproTech) for 30 min. Cells were fixed with 4% paraformaldehyde-PBS at 4°C for 10 min and permeabilized with 0.5% Triton X-100 and 5 mM EDTA in 50 mM Tris-HCl/150 mM NaCl buffer. After blocking with 3% BSA-PBS, cells were stained with Abs against anti-GFP (598 or RQ2; MBL) and anti-p65 (A or F-6; Santa Cruz). Nuclear DNA was stained with DAPI (DAPI; Sigma). The specimens were examined using an FV1200 (Olympus) confocal microscope.

Statistical analysis

GraphPad Prism 6 was used for statistical analyses. The means of two groups were compared by the unpaired Student *t* test. The Mann–Whitney *U* test was used to compare nonparametric datasets. The p values <0.05 were considered statistically significant.

Results

Defective formation of T cell area in SLOs of Ccl19-IκBSR mice

To assess the impact of FSC-specific inactivation of the canonical NF-κB pathway in vivo, we first generated a mouse strain bearing the transgene, CAG promoter, and a bicistronic expression cassette encoding *IκBSR-ires-EGFP* interrupted with a transcription termination signal held between two loxP sites, which was knocked in to the *Rosa26* locus (*R26-stop^{flox}-IκBSR*) (Fig. 1A). This strain was further crossed with *Ccl19-Cre* BAC transgenic mouse to obtain animals that had both transgenic alleles (*Ccl19-IκBSR*) in which constitutive IκBSR expression was expectedly induced in SLO FSCs that were expressing or had once expressed the *Ccl19* gene. We hypothesized that SLOs may disappear in such mice if the activity of the canonical NF-κB pathway in mesenchymal stromal cells, especially in fetal LTo cells, was essential for SLO development. However, virtually all LNs developed in *Ccl19-IκBSR* mice, although they were apparently

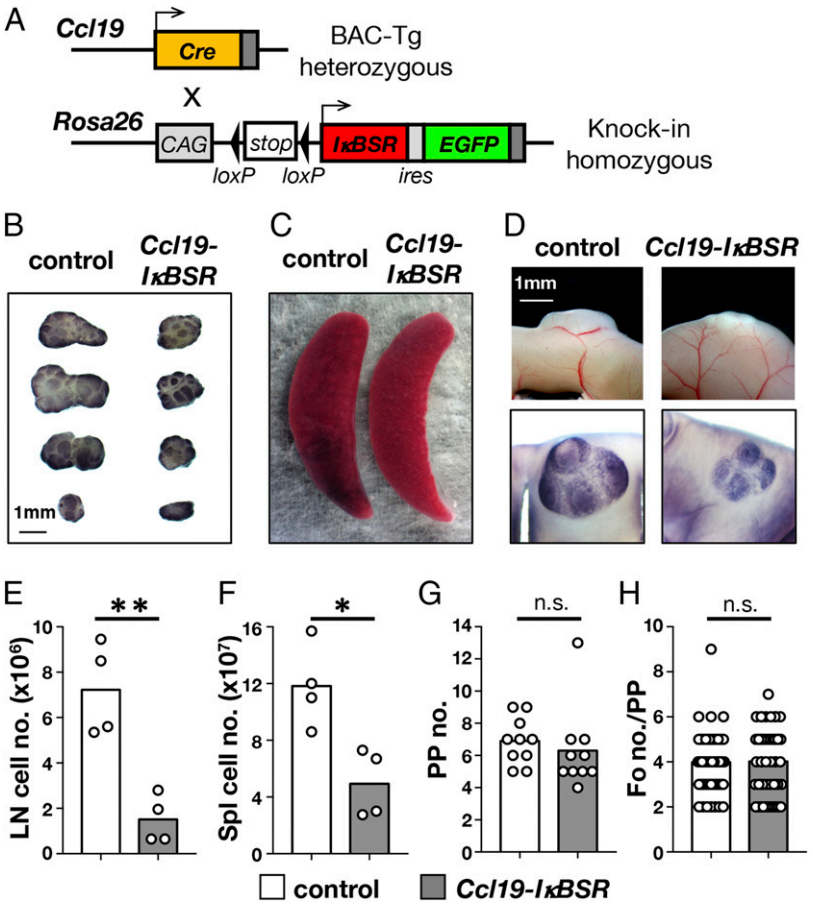

FIGURE 1. Hypoplastic SLOs in *Ccl19-IκBSR* mice. (**A**) Strategy for the conditional inactivation of the canonical NF-κB pathway specific to FSCs in SLOs. (**B**) Whole-mount B220 staining of isolated LNs. From the top, axillary, brachial, inguinal, and popliteal LNs. (**C**) Macroscopic view of the spleens. (**D**) Macroscopic side view of PPs (upper) and after whole-mount B220 staining of the same PPs (lower). Images of organs are the representatives of SLOs from more than five mice. (**E** and **F**) The numbers of cells in the LNs [(E), pooled pair of axillary, brachial, and inguinal LNs] and the spleen (F). Circles represent data from individual mice, and the bar represents the mean. (**G** and **H**) The number of PPs in the small intestine (G) and the number of follicles in a single PP (H). $*p < 0.05$, $**p < 0.005$. n.s., not significant.

hypoplastic with smaller organ sizes and morphological abnormalities compared with their appearance in control animals (*R26-stop^{flox}-IκBSR*). In fact, the total cell number was markedly lower in LNs from *Ccl19-IκBSR* mice (Fig. 1B, 1E). The size and morphology of the spleen were comparable to those in control mice; however, the total spleen cell number was significantly reduced in *Ccl19-IκBSR* animals (Fig. 1C, 1F). It was also evident that the development of PPs was incomplete, although the numbers of PPs in the small intestine and of the follicles in a single PP were normal (Fig. 1D, 1G, 1H).

To determine the cause of these morphological abnormalities of SLOs in *Ccl19-IκBSR* mice, we next examined tissue structures in greater detail by fluorescence immunohistochemistry. The most remarkable alteration in each SLO was the defective formation of the T cell area (Fig. 2). In the paracortex of LNs, the accumulation of T cells was dramatically reduced in accordance with the diminished T cell proportion in total LN cells compared with that in controls (Fig. 2A, 2D). In contrast, the number of B cells was proportionally higher, and follicular B cell accumulations were clearly formed in the outer cortex, albeit with somewhat disordered morphology. PNAd$^+$ high endothelial venules (HEVs) were present, and the expansion of the medullary sinus was evident in *Ccl19-IκBSR* LNs. In the spleen, T cell localization, especially in the periarteriolar lymphoid sheath, the T cell area in the white pulp, was severely affected in *Ccl19-IκBSR* mice in sharp contrast to the follicle-like B cell accumulations (Fig. 2B). The T cell–B cell ratio in the whole spleen was unaltered likely due to the mislocalization of T cells mainly in the red pulp instead of the white pulp (Fig. 2B, 2E). The interfollicular T cell area was nearly absent in PPs of *Ccl19-IκBSR* mice, whereas formed follicles were smaller but relatively substantial compared with those in controls (Fig. 2C). Follicular B cell area and CD35$^+$ FDC networks were clearly formed in all SLOs of *Ccl19-IκBSR* mice (Supplemental Fig. 1A). RANKL^{+-} MAdCAM-1$^+$ MRCs were also detected in the outer margin of follicles beneath the subcapsular sinus in LNs (Supplemental Fig. 1B). Thus, in contrast to T cell area, follicular structures and associated FSC subsets developed appropriately in the *Ccl19-IκBSR* environment.

Defect of TRC development in SLOs of Ccl19-IκBSR mice

Given the defective formation of the T cell area in SLOs from *Ccl19-IκBSR* mice, the conditional inhibition of NF-κB activation was assumed to affect the subset of FSCs in this area. Thus, we next checked the expression of CCL21, a typical hallmark of TRCs. In normal LN sections, an anti-CCL21 Ab strongly stained reticular TRCs as well as endothelial cells in HEVs. In contrast, the CCL21 signal was dramatically reduced in *Ccl19-IκBSR* LNs; only faint expression was detected in HEVs (Fig. 3A). CCL21 expression was nearly absent in the white pulp of the spleen as well (Fig. 3B). CXCL13 expression in *Ccl19-IκBSR* LNs was comparable to that in control, whereas follicular stromal cells in the spleen of *Ccl19-IκBSR* animals showed substantial but somewhat disarranged pattern of CXCL13 expression (Fig. 3A, 3B). Quantitative PCR analysis demonstrated dramatically diminished expression of the *Ccl19* and *Ccl21a* genes in *Ccl19-IκBSR* LNs, whereas *Cxcl13* expression showed an inversely correlated increase, probably due to the relatively augmented proportion of CXCL13-expressing cells in the total population of LN cells (Fig. 3C). Likewise, expression of CCL19 and CCL21a was nearly abolished in *Ccl19-IκBSR* spleen, whereas CXCL13 expression was only slightly decreased

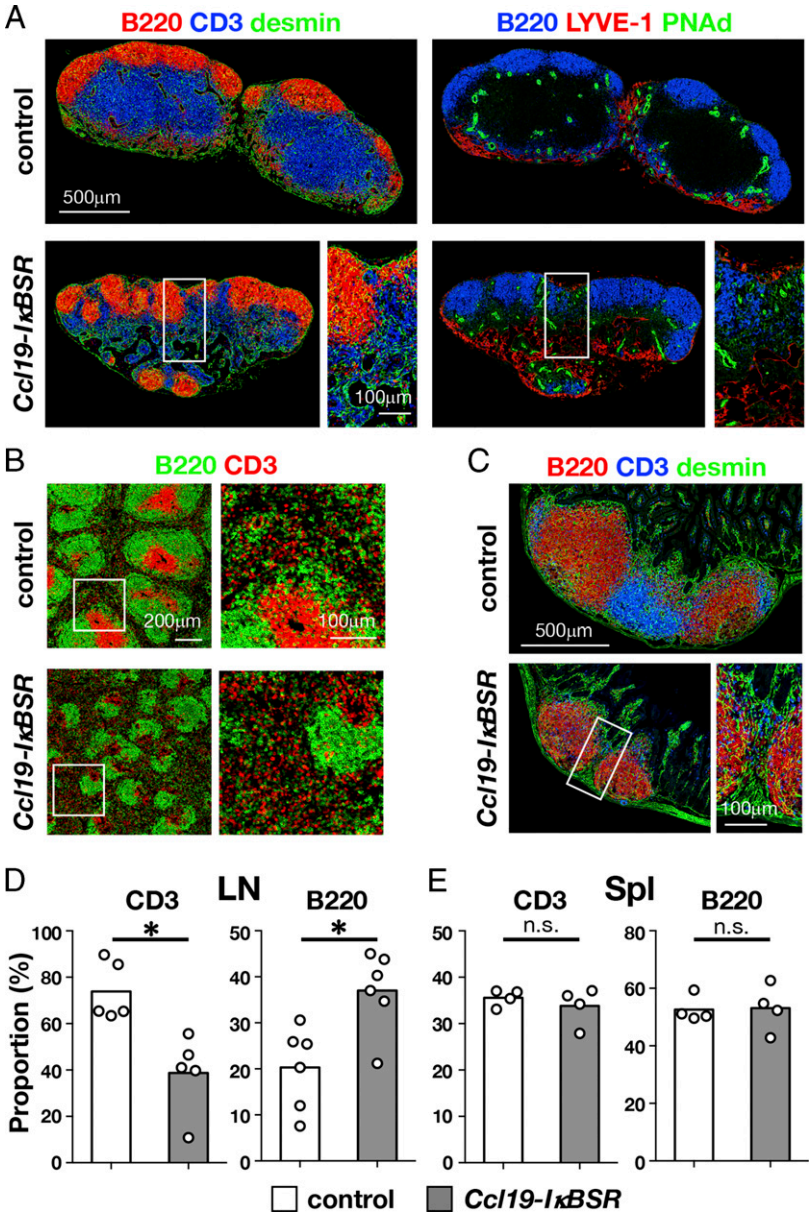

FIGURE 2. Defective development of T cell area in SLOs *of Ccl19-IκBSR* mice. (**A**–**C**) Confocal immunohistochemistry of LNs (A), spleen (B), and PPs (C). Boxed regions are magnified in the panels on the right. Images of tissues are the representatives of SLOs from four mice. (**D** and **E**) Proportions of T cells and B cells in LNs [(D), pooled axillary, brachial, and inguinal LNs] and the spleen (E) determined by flow cytometry. Circles represent data from individual mice, and the bar represents the mean. *$p < 0.01$. n.s., not significant.

compared with that in control (Fig. 3D), which was consistent with immunohistochemical observations. Accordingly, these findings indicate that conditional inactivation of the canonical NF-κB pathway under the control of *Ccl19* expression led to a selective loss of TRCs in SLOs.

To determine if the deficiency of TRC and decrement of lymphocytes of *Ccl19-IκBSR* mice were also observed in developing LNs, we examined tissues from neonates (1 wk) and young (2 and 4 wk of age) mice. We found that the total LN number, especially in 2 and 4 wk after birth, was markedly reduced in *Ccl19-IκBSR* mice compared with that in control animals, whereas no significant difference was observed in the numbers of neonatal LNs in mutant and control animals (Supplemental Fig. 2A). $CCL21^+$ FSCs were already virtually absent in neonatal as well as young *Ccl19-IκBSR* mice, whereas CCL21-producing stromal network was clearly formed in T cell area of neonatal LNs in control mice (Supplemental Fig. 2B). Therefore, these observations suggest that the differentiation of TRCs is inhibited in the early stages of development, most likely immediately after the expression of *Ccl19-Cre*, which induces IκBSR and blocks NF-κB signaling.

Requirement for the activation of the canonical NF-κB pathway in distinct differentiation programs of FSC subsets

Although the expression of *Ccl19* is a typical feature of TRCs, LTo cells in fetal anlagen, from which all adult type FSC subsets are supposed to differentiate, also expressed this gene, and, in fact, *Ccl19-Cre* has shown functional expression from this stage (33). Therefore, it was puzzling that the conditional inactivation of NF-κB under the control of *Ccl19-Cre* showed a selective effect on TRCs. In particular, in a clear contradiction to this finding, the development of FDC network has been suggested to require NF-κB pathways (9, 31). Most FSCs, including follicular subsets, actually displayed EYFP expression in *Ccl19-Cre/R26-stop^{flox}-EYFP* (*Ccl19-EYFP*) simple fate mapping system (Fig. 4A–C) (30), demonstrating that MRCs and FDCs, in addition to TRCs, had once expressed *Ccl19* gene during development. In adult *Ccl19-Cre* mice, Cre-expressing cells were in fact detected in the paracortex but not in the follicles (Supplemental Fig. 3A). These observations support the notion that the *Ccl19* gene is transiently expressed in the precursor of follicular FSCs and subsequently becomes downregulated during the course of their differentiation.

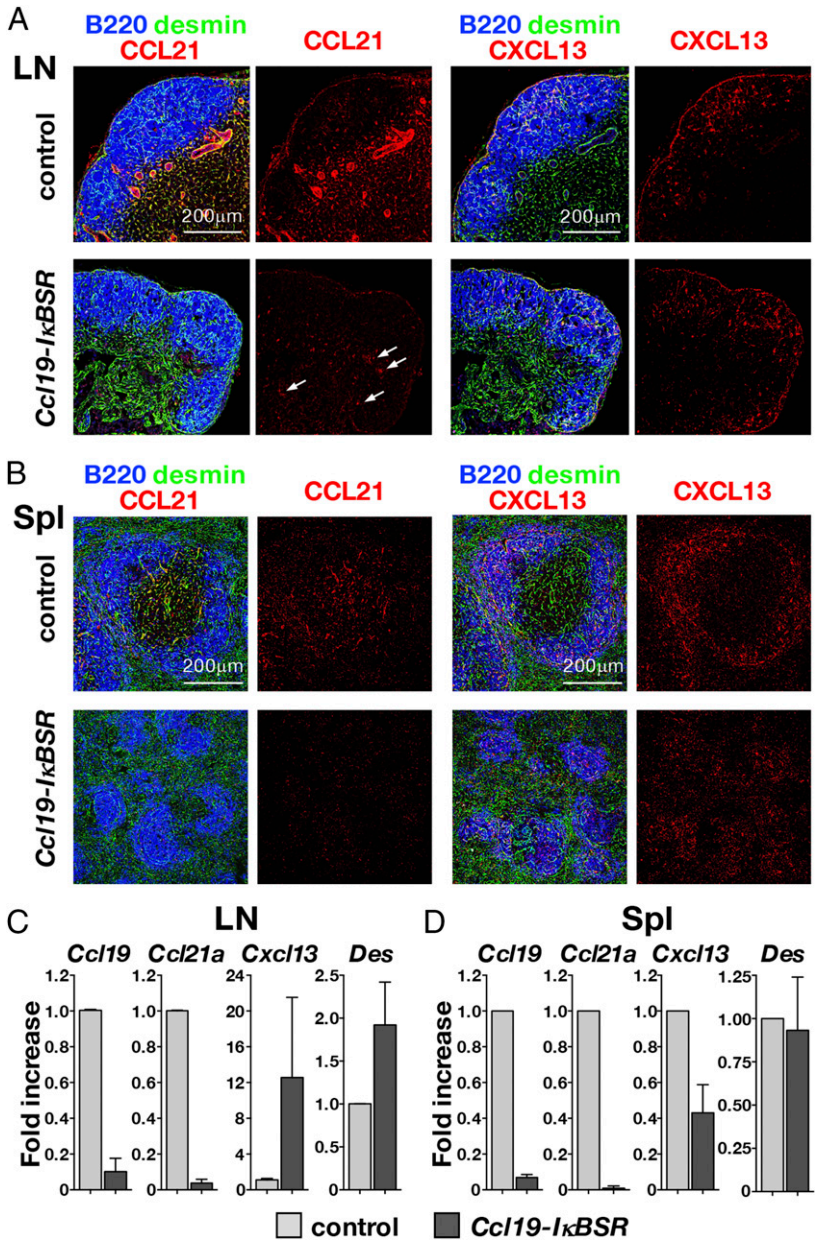

FIGURE 3. Defective development of TRCs in SLOs of *Ccl19-IκBSR* mice. (**A** and **B**) Confocal immunohistochemical staining for CCL21 or CXCL13 in LNs (A) and the spleen (B). Arrows indicate lower expression of CCL21 in HEVs. Images of tissues are the representatives of SLOs from four mice. (**C** and **D**) Quantitative RT-PCR analysis for the expression of *Ccl19*, *Ccl21a*, *Cxcl13*, and *Des* (desmin) genes in LNs (C) and the spleen (D). Data are presented as the mean ± SD ($n \geq 3$).

To identify IκBSR-expressing cells in SLOs of *Ccl19-IκBSR* mice, we took advantage of detecting bicistronic EGFP expression. Interestingly, $EGFP^+$ cells were detected only in a small fraction of mesenchymal cells in the perifollicular and medullary regions, especially in the perivascular area, of LNs (Fig. 4A, 4B arrows), whereas the majority of FSCs were devoid of EGFP expression. Flow cytometry analysis of enzymatically digested LNs also supported that observation, as only a limited cell population (<10%) showed EGFP signal in $CD45^-CD31^-$podoplanin$^+$ stromal fraction (Fig. 4C). Notably, EGFP was almost undetectable in follicular stromal cells, showing that these cells did not express (and, in fact, had never expressed) *Ccl19-Cre* (i.e., IκBSR). Likewise, fluorescence signal was absent in follicle-like B cell accumulations in the spleen, whereas a fraction of stromal cells in perivascular regions outside the follicles and in the red pulp exhibited EGFP expression (Supplemental Fig. 3B). We confirmed that cultured primary FSCs expressing EGFP from *Ccl19-IκBSR* mice did not exhibit the nuclear translocation of RelA(p65) upon TNF-α stimulation, showing that IκBSR in fact blocked the activation of canonical NF-κB pathway in the target cells (Supplemental Fig. 4). Taken together, TRCs were essentially absent, whereas no MRCs and FDCs expressing IκBSR were present in *Ccl19-IκBSR* mice.

Discussion

Detailed observations of tissue structures in *Ccl19-IκBSR* mice SLOs in this study suggest that the differentiation or maintenance of all FSC subsets, namely TRCs, MRCs, and FDCs, requires canonical NF-κB activation. To explain the outcome of conditional NF-κB inactivation in FSCs driven by *Ccl19-Cre*, we propose a speculative model of the developmental program of FSC subsets in normal and IκBSR-expressing condition (Fig. 4D). As *Ccl19* expression is a hallmark of TRCs, it is a reasonable consequence that *Ccl19*-driven induction of IκBSR straightforwardly suppressed TRC differentiation through the inhibition of the canonical NF-κB pathway. In normal conditions, MRCs and FDCs are likely to exhibit transient expression of *Ccl19* at progenitor level in fetal anlagen or postnatal period, which would be the reason why most follicular FSCs were marked with EYFP expression in *Ccl19-EYFP* fate mapping system. In *Ccl19-IκBSR* mice, in contrast, transient

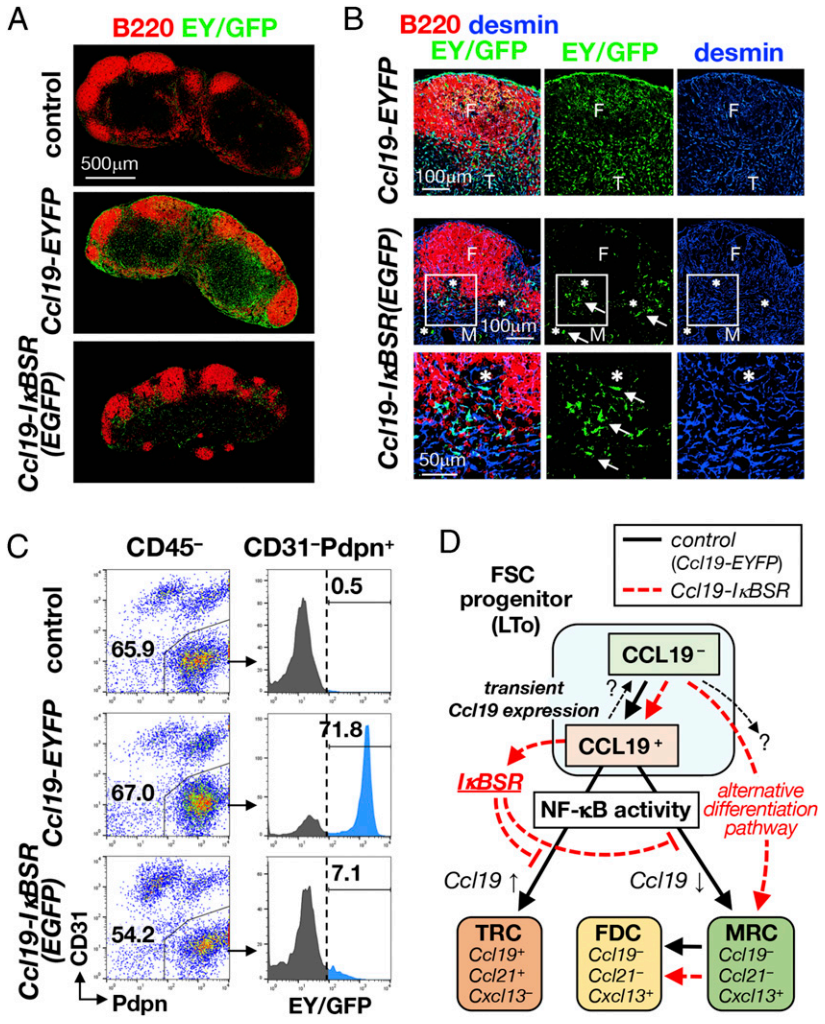

FIGURE 4. Defect in the differentiation of FSC subsets and rescued follicular stroma in SLOs of *Ccl19-IκBSR* mice. (**A**) Detection of EYFP- or EGFP-expressing cells in LNs by confocal immunohistochemistry. Images of tissues are the representatives of LNs from three mice (more than six LNs each). (**B**) Distribution of EYFP- or EGFP-expressing cells in the LNs. Boxed perifollicular regions are magnified in the bottom panels. Note that the clusters of EGFP-expressing FSCs are detected in the perivasucular and medullary regions (arrows). Asterisks indicate blood vessels. Images of tissues are the representatives of more than three mice. (**C**) Proportion of EYFP- or EGFP-expressing cells in $CD45^{-}CD31^{-}$ podoplanin $(Pdpn)^{+}$ LN stromal cell fraction determined by flow cytometry. Typical results representative of three independent experiments are shown. Numbers indicate the percentage of $CD31^{-}Pdpn^{+}$ fraction in $CD45^{-}$ cells (left dot plots) and EY/GFP^{+} fraction in $CD31^{-}Pdpn^{+}$ cells (right histograms, light blue parts). (**D**) A model of the differentiation of FSC subsets in normal (black arrows) or NF-κB–inactivated condition (red dotted arrows). F, follicle; M, medulla; T, T cell area.

Ccl19-Cre expression and subsequent NF-κB inactivation in FSC progenitors likely suppressed the development of MRCs (and following FDCs), as virtually none of these cells expressed EGFP (and IκBSR). $IκBSR^{-}$ follicular stromal cells present in adult *Ccl19-IκBSR* SLOs likely derived from a small number of $CCL19^{-}$ cells that had circumvented transient CCL19 expression but had a potential to substitute the follicular area. Such a compensatory development of follicles in *Ccl19-IκBSR* SLOs resulted in the similarity of the whole tissue structure to that of *plt* mice that lack T cell area because of the absence of *Ccl19* and *Ccl21a* genes (37). The alternative differentiation pathway could possibly take place in normal setting, as $EYFP^{-}$ FSCs were constantly detected in the LNs of adult *Ccl19-EYFP* mice. $EGFP^{+}$ cells still present in *Ccl19-IκBSR* SLOs were possibly 1) unusual cells that could not differentiate to mature FSCs, 2) FSC subsets that did not require NF-κB activity for their differentiation, or 3) cells preserving undifferentiated state (equivalent to that of progenitors) in adult SLOs. Transient expression of *Ccl19* gene and the existence of $EYFP^{-}$ FSCs suggest the presence of a stochastic state in terms of chemokine expression in FSC progenitor cells. During that period, direct contact with lymphoid cells and/or other hematopoietic cells might fix the characteristics of FSCs to a particular subset and facilitate the localization of hematopoietic cells to construct tissue subcompartments in a manner of a positive feedback loop or self-organization.

The conclusion that all three FSC subsets require the activation of the NF-κB canonical pathway in their differentiation was drawn from the conditional induction of NF-κB suppressor coupled with a fate mapping system that visualized targeted cells. However, because the expression of noncanonical NF-κB components such as *Relb* and *Nfkb2* depend on canonical NF-κB activity to some extent and IκBSR is in fact known to inhibit both pathways (13–15), the phenotypes observed in *Ccl19-IκBSR* mice are considered to be a consequence of whole NF-κB suppression in FSCs. In addition, potential limitations or uncertainties are inevitable in a conditional gene induction system in vivo. The expression levels of fluorescent reporter proteins induced by cell type–specific Cre recombinases do not always correlate with the corresponding deletion/recombination of another gene of interest. In our system, IκBSR may not express efficiently in any of the $CCL19^{+}$ FSCs or not block NF-κB activation completely. These are the future issues that should be verified by using complementary approaches. Furthermore, the conditional ablation of genes that are essential for the differentiation and maintenance of cells that use *Ccl19-Cre* system need a careful consideration because the compensatory substitution of FSCs could derive from $CCL19^{-}$ progenitors. Consequently, we cannot yet exclude a possibility that NF-κB activity in LTo cells or FSC progenitors is essential for SLO development, as alternatively differentiated FSCs with intact NF-κB signaling could promote early organogenesis in *Ccl19-IκBSR* mice.

Acknowledgments

We thank Changchun Xiao for CTV targeting vector.

Disclosures

The authors have no financial conflicts of interest.

References

1. Randall, T. D., D. M. Carragher, and J. Rangel-Moreno. 2008. Development of secondary lymphoid organs. *Annu. Rev. Immunol.* 26: 627–650.
2. Roozendaal, R., and R. E. Mebius. 2011. Stromal cell-immune cell interactions. *Annu. Rev. Immunol.* 29: 23–43.
3. Mebius, R. E., P. Rennert, and I. L. Weissman. 1997. Developing lymph nodes collect CD4+CD3- LTbeta+ cells that can differentiate to APC, NK cells, and follicular cells but not T or B cells. *Immunity* 7: 493–504.
4. Yokota, Y., A. Mansouri, S. Mori, S. Sugawara, S. Adachi, S. Nishikawa, and P. Gruss. 1999. Development of peripheral lymphoid organs and natural killer cells depends on the helix-loop-helix inhibitor Id2. *Nature* 397: 702–706.
5. Honda, K., H. Nakano, H. Yoshida, S. Nishikawa, P. Rennert, K. Ikuta, M. Tamechika, K. Yamaguchi, T. Fukumoto, T. Chiba, and S. I. Nishikawa. 2001. Molecular basis for hematopoietic/mesenchymal interaction during initiation of Peyer's patch organogenesis. *J. Exp. Med.* 193: 621–630.
6. Mebius, R. E. 2003. Organogenesis of lymphoid tissues. [Published erratum appears in 2003 *Nat. Rev. Immunol.* 3: 509.] *Nat. Rev. Immunol.* 3: 292–303.
7. Mebius, R. E., and G. Kraal. 2005. Structure and function of the spleen. *Nat. Rev. Immunol.* 5: 606–616.
8. Schaeuble, K., M. R. Britschgi, L. Scarpellino, S. Favre, Y. Xu, E. Koroleva, T. K. A. Lissandrin, A. Link, M. Matloubian, C. F. Ware, et al. 2017. Perivascular fibroblasts of the developing spleen act as LTα1β2-dependent precursors of both T and B zone organizer cells. *Cell Rep.* 21: 2500–2514.
9. Alcamo, E., N. Hacohen, L. C. Schulte, P. D. Rennert, R. O. Hynes, and D. Baltimore. 2002. Requirement for the NF-kappaB family member RelA in the development of secondary lymphoid organs. *J. Exp. Med.* 195: 233–244.
10. Weih, F., and J. Caamaño. 2003. Regulation of secondary lymphoid organ development by the nuclear factor-kappaB signal transduction pathway. *Immunol. Rev.* 195: 91–105.
11. Yilmaz, Z. B., D. S. Weih, V. Sivakumar, and F. Weih. 2003. RelB is required for Peyer's patch development: differential regulation of p52-RelB by lymphotoxin and TNF. *EMBO J.* 22: 121–130.
12. Carragher, D., R. Johal, A. Button, A. White, A. Eliopoulos, E. Jenkinson, G. Anderson, and J. Caamaño. 2004. A stroma-derived defect in NF-kappaB2-/- mice causes impaired lymph node development and lymphocyte recruitment. *J. Immunol.* 173: 2271–2279.
13. Dejardin, E., N. M. Droin, M. Delhase, E. Haas, Y. Cao, C. Makris, Z. W. Li, M. Karin, C. F. Ware, and D. R. Green. 2002. The lymphotoxin-beta receptor induces different patterns of gene expression via two NF-kappaB pathways. *Immunity* 17: 525–535.
14. Basak, S., V. F. Shih, and A. Hoffmann. 2008. Generation and activation of multiple dimeric transcription factors within the NF-kappaB signaling system. *Mol. Cell. Biol.* 28: 3139–3150.
15. Suto, H., T. Katakai, M. Sugai, T. Kinashi, and A. Shimizu. 2009. CXCL13 production by an established lymph node stromal cell line via lymphotoxin-beta receptor engagement involves the cooperation of multiple signaling pathways. *Int. Immunol.* 21: 467–476.
16. Bonizzi, G., M. Bebien, D. C. Otero, K. E. Johnson-Vroom, Y. Cao, D. Vu, A. G. Jegga, B. J. Aronow, G. Ghosh, R. C. Rickert, and M. Karin. 2004. Activation of IKKalpha target genes depends on recognition of specific kappaB binding sites by RelB:p52 dimers. *EMBO J.* 23: 4202–4210.
17. Onder, L., U. Morbe, N. Pikor, M. Novkovic, H. W. Cheng, T. Hehlgans, K. Pfeffer, B. Becher, A. Waisman, T. Rulicke, et al 2017. Lymphatic endothelial cells control initiation of lymph node organogenesis. *Immunity* 47: 80–92.e4.
18. Mueller, S. N., and R. N. Germain. 2009. Stromal cell contributions to the homeostasis and functionality of the immune system. *Nat. Rev. Immunol.* 9: 618–629.
19. Cyster, J. G. 2010. B cell follicles and antigen encounters of the third kind. *Nat. Immunol.* 11: 989–996.
20. Ansel, K. M., V. N. Ngo, P. L. Hyman, S. A. Luther, R. Förster, J. D. Sedgwick, J. L. Browning, M. Lipp, and J. G. Cyster. 2000. A chemokine-driven positive feedback loop organizes lymphoid follicles. *Nature* 406: 309–314.
21. Katakai, T., H. Suto, M. Sugai, H. Gonda, A. Togawa, S. Suematsu, Y. Ebisuno, K. Katagiri, T. Kinashi, and A. Shimizu. 2008. Organizer-like reticular stromal cell layer common to adult secondary lymphoid organs. *J. Immunol.* 181: 6189–6200.
22. Jarjour, M., A. Jorquera, I. Mondor, S. Wienert, P. Narang, M. C. Coles, F. Klauschen, and M. Bajénoff. 2014. Fate mapping reveals origin and dynamics of lymph node follicular dendritic cells. *J. Exp. Med.* 211: 1109–1122.
23. Krautler, N. J., V. Kana, J. Kranich, Y. Tian, D. Perera, D. Lemm, P. Schwarz, A. Armulik, J. L. Browning, M. Tallquist, et al. 2012. Follicular dendritic cells emerge from ubiquitous perivascular precursors. *Cell* 150: 194–206.
24. Luther, S. A., H. L. Tang, P. L. Hyman, A. G. Farr, and J. G. Cyster. 2000. Coexpression of the chemokines ELC and SLC by T zone stromal cells and deletion of the ELC gene in the plt/plt mouse. *Proc. Natl. Acad. Sci. USA* 97: 12694–12699.
25. Link, A., T. K. Vogt, S. Favre, M. R. Britschgi, H. Acha-Orbea, B. Hinz, J. G. Cyster, and S. A. Luther. 2007. Fibroblastic reticular cells in lymph nodes regulate the homeostasis of naive T cells. *Nat. Immunol.* 8: 1255–1265.
26. Katakai, T., T. Hara, M. Sugai, H. Gonda, and A. Shimizu. 2004. Lymph node fibroblastic reticular cells construct the stromal reticulum via contact with lymphocytes. *J. Exp. Med.* 200: 783–795.
27. Katakai, T., T. Hara, J. H. Lee, H. Gonda, M. Sugai, and A. Shimizu. 2004. A novel reticular stromal structure in lymph node cortex: an immuno-platform for interactions among dendritic cells, T cells and B cells. *Int. Immunol.* 16: 1133–1142.
28. Castagnaro, L., E. Lenti, S. Maruzzelli, L. Spinardi, E. Migliori, D. Farinello, G. Sitia, Z. Harrelson, S. M. Evans, L. G. Guidotti, et al. 2013. Nkx2-5(+)islet1(+) mesenchymal precursors generate distinct spleen stromal cell subsets and participate in restoring stromal network integrity. *Immunity* 38: 782–791.
29. Katakai, T. 2012. Marginal reticular cells: a stromal subset directly descended from the lymphoid tissue organizer. *Front. Immunol.* 3: 200.
30. Tumanov, A. V., S. I. Grivennikov, A. N. Shakhov, S. A. Rybtsov, E. P. Koroleva, J. Takeda, S. A. Nedospasov, and D. V. Kuprash. 2003. Dissecting the role of lymphotoxin in lymphoid organs by conditional targeting. *Immunol. Rev.* 195: 106–116.
31. Victoratos, P., J. Lagnel, S. Tzima, M. B. Alimzhanov, K. Rajewsky, M. Pasparakis, and G. Kollias. 2006. FDC-specific functions of p55TNFR and IKK2 in the development of FDC networks and of antibody responses. *Immunity* 24: 65–77.
32. Matsumoto, M., Y. X. Fu, H. Molina, G. Huang, J. Kim, D. A. Thomas, M. H. Nahm, and D. D. Chaplin. 1997. Distinct roles of lymphotoxin alpha and the type I tumor necrosis factor (TNF) receptor in the establishment of follicular dendritic cells from non-bone marrow-derived cells. *J. Exp. Med.* 186: 1997–2004.
33. Chai, Q., L. Onder, E. Scandella, C. Gil-Cruz, C. Perez-Shibayama, J. Cupovic, R. Danuser, T. Sparwasser, S. A. Luther, V. Thiel, et al. 2013. Maturation of lymph node fibroblastic reticular cells from myofibroblastic precursors is critical for antiviral immunity. *Immunity* 38: 1013–1024.
34. Wrighton, C. J., R. Hofer-Warbinek, T. Moll, R. Eytner, F. H. Bach, and R. de Martin. 1996. Inhibition of endothelial cell activation by adenovirus-mediated expression of I kappa B alpha, an inhibitor of the transcription factor NF-kappa B. *J. Exp. Med.* 183: 1013–1022.
35. Thai, T. H., D. P. Calado, S. Casola, K. M. Ansel, C. Xiao, Y. Xue, A. Murphy, D. Frendewey, D. Valenzuela, J. L. Kutok, et al. 2007. Regulation of the germinal center response by microRNA-155. *Science* 316: 604–608.
36. Katakai, T., N. Kondo, Y. Ueda, and T. Kinashi. 2014. Autotaxin produced by stromal cells promotes LFA-1-independent and Rho-dependent interstitial T cell motility in the lymph node paracortex. *J. Immunol.* 193: 617–626.
37. Gunn, M. D., S. Kyuwa, C. Tam, T. Kakiuchi, A. Matsuzawa, L. T. Williams, and H. Nakano. 1999. Mice lacking expression of secondary lymphoid organ chemokine have defects in lymphocyte homing and dendritic cell localization. *J. Exp. Med.* 189: 451–460.